JOURNAL OF MATERIALS SCIENCE 30 (1995) 4355–4362

Impure zirconia electrical conductivity enhancement by rare-earth minority ions in the Y_2O_3 RE_2O_3 ZrO_2 system

D. P. F. DE SOUZA, A. L. CHINELATTO
Department of Materials Engineering, UFSCar., 13 565-905-S. Carlos-SP, Brazil
M. F. DE SOUZA
Department of Physics and Materials Science,IFQSC-USP, 13 560-250-S. Carlos-SP, Brazil

Impure zirconia stabilized by 12 wt% yttria concentrate (85 wt% Y_2O_3 + 15 wt% rare-earth (RE)) was found to have high grain and grain-boundary electrical conductivities. The influence of the RE on the segregation of impurities was studied for four different compositions. Microstructure features are evidence for the enhanced segregation of impurities due to RE ions. The increased grain and grain-boundary conductivities are a consequence of the segregation of impurities.

1. Introduction

Zirconia electrolytes have been extensively investigated in regard to their electrical properties [1–20], the influence of sintering aids on conductivity [21–31], the microstructure development of cubic, tetragonal, and partially stabilized zirconia [32–41], and their stabilization by ions of several ionic radii [1, 2, 11, 13–15, 42]. Yttrium is the element most commonly used to stabilize the cubic and tetragonal phases, but rare-earths (RE) and the combination yttrium–RE have also been used [1, 15, 27, 43]. Studies of impure electrolytes stabilized by RE-ions or the combination RE + Y ions are few and do not correlate microstructure with electrical properties [1, 15, 21, 27].

The electrical conductivity of zirconia electrolytes in the temperature range 200–1000 °C is known to be ionic in nature. The total conductivity, σ_t, can be divided in two parts – the grain conductivity, σ_g, and the grain-boundary conductivity, σ_{gb}. These conductivities are differently influenced by such parameters as impurities, grain size, and ionic radius of the stabilizing ion. Generally, σ_g behaves as follows: (1) σ_g has its maximum value at ~8 mol % concentration of the stabilizing ion [3, 5, 9, 15]; (2) E_g, the activation energy for σ_g, increases with the concentration of the stabilizing ion without discontinuity going from the tetragonal to the cubic phase [9]; (3) grain size has no effect on σ_g nor E_g [33]; (4) on decreasing the ionic radius of the stabilizing ion, σ_g increases and E_g decreases [2]; (5) impurities decrease σ_g (the effect of silica is more pronounced than Al_2O_3 when these impurities are dissolved in the lattice [8, 25]). Earlier works have considered that Al^{3+} dissolved in the matrix would increase σ_g [22, 23]. Butler and Drennan [27] found that Al_2O_3 acts as a scavenger for SiO_2. This is one possible reason for the observed increase in the conductivity of the Al_2O_3-doped electrolytes in these early works once silica is the most common zirconia impurity. The grain-boundary conductivity, σ_{gb}, behaves as follows: (1) σ_{gb} is very sensitive to impurities [26, 33] and it may change from $2.6 \times 10^{-3}\,\Omega^{-1}\,cm^{-1}$ in a pure sample to $3.2 \times 10^{-4}\,\Omega^{-1}\,cm^{-1}$ in a 1 wt % SiO_2-doped sample [8]; (2) E_{gb}, the activation energy for σ_{gb}, is higher than E_g by as much as 0.15 eV in pure samples [33]; (3) σ_{gb} increases with increasing grain size [33]; (4) impurities such as SiO_2, Fe_2O_3, Cr_2O_3, and Al_2O_3 increase the electrolyte sinterability but reduce σ_{gb} as well as σ_g [26, 28, 29, 31]. The influence of 0.4 mol % alumina on σ_{gb} is 2.3 times larger than on σ_g [25]; (5) Badwal and Drennan [34], studying a high-purity electrolyte with low silica level (20 p.p.m), found that at temperatures below 1500 °C it was dispersed along the grain boundaries but when sintered at higher temperatures, it moved to pockets along the grain boundaries; (6) the influence of stabilizing ions of low ionic radii, such as Sc^{3+} and Yb^{3+} on σ_{gb} has been mentioned but not considered in a systematic way [1, 11, 15, 27, 45]. The presence of silica in the grain boundary allows the formation of a glassy phase. This was considered by Chaim *et al.* [40] and by Butler and Heuer [39] to be necessary to explain the formation of a narrow cubic zone around the growing grain in PSZ ceramics.

In this work, a 99% pure commercial zirconia was stabilized by ~6 mol % Y_2O_3 and 0.6 mol % RE_2O_3 producing PSZ samples. The influence of the RE on the microstructure and on the electrical behaviour was observed and is discussed. Cost reduction for producing conductive eletrolytes and the availability of the yttria concentrates were the starting points for this investigation.

0022–2461

2. Experimental procedure

The starting materials for compositions preparation were 99% pure zirconia and concentrates of yttrium carbonates with 75% and 85% yttria concentration as shown in Table I. High-purity yttria, dysprosia, and erbia, 99.9% (Molicorp Corporation, USA) were used to prepare comparison compositions denominated 1, 2, and 3, respectively. The compositions studied are shown in Table II. Composition 4 was prepared having 12 wt % of equivalent oxides from the 75%-rich yttria concentrate, while composition 5 was prepared in the same way but from the 85%-rich yttria concentrate. Compositions 6 and 7 were prepared like composition 5 but with 8 and 10 wt %, respectively, of the yttria concentrate in order to determine the minimum concentration of stabilizing ions necessary to have monoclinic phase free samples.

Compositions preparation followed standard procedures. The powders were first milled, dried and calcined to convert the carbonates to oxides and milled again, using zirconia balls, to 0.7 μm average particle size. After spray drying, the powders were isostatically pressed at 270 MPa in to discs of 13 mm diameter, sintered for 8 h at 1600 °C in air and cooled to room temperature at a rate of 500 °C h^{-1}. From each composition, at least 20 discs were prepared. The density of the discs was measured to an accuracy of 10^{-3} g cm^{-3} using Archimedes' method with distilled water as the immersion medium. X-ray diffraction and dilatometry were used to study the crystalline phases after sintering. Samples for observation of microstructures were ground with successively finer grades of SiC papers, polished successively with 6, 3 and 1 μm diamond paste, and finished with 0.3 μm alumina slurry, and then thermally etched at 1550 °C for 5 min. Optical microscopy using sodium light and shadow effects, scanning electron microscopy (SEM), and energy dispersive spectrometry (EDS) qualitative analysis were used in this work. Electrical conductivity measurements were done using an HP 4592A LP impedance analyser in the frequency range 10 Hz to 13 MHz. The grain, σ_g, grain boundary, σ_{gb}, and total σ_t, conductivities, were obtained by analysis of the impedance spectra of each sample through the computer program "Equivalent Circuit" [44]. The discs for electrical measurements had platinum electrodes in both faces obtained by applying a platinum paint (308A Demetron, Germany) on their polished surfaces and baking them at 1100 °C for 30 min.

3. Results and Discussion

3.1. Crystalline phase

Sample compositions, described in Table II, have a total molar concentration of stabilizing ions (Y + RE) near 6.5% with the exception of composition 1 which

TABLE I Chemical composition of the oxides (wt %)

	Y_2O_3	La_2O_3	Ce_2O_3	Gd_2O_3	Tb_2O_3	Dy_2O_3	Ho_2O_3	Er_2O_3	Yb_2O_3
Yttria A[a]	75.20	0.10	0.40	1.00	1.40	13.80	2.10	4.50	1.40
Yttria B[a]	85.80	0.30	0.65	0.25	0.10	3.80	2.50	6.00	0.40
	ZrO_2	HfO_2	SiO_2	Al_2O_3	Fe_2O_3	TiO_2			
Zirconia[b]	97.40	2.06	0.20	0.45	0.02	0.13			

[a] Nuclemon, Brazil.
[b] TAM Ceramics, USA.

TABLE II Percentage of oxides (mol %) in the studied compositions

	Composition					
Oxides	1	2	3	4	5	6
ZrO_2	90.830	91.220	91.260	91.460	91.180	92.310
HfO_2	1.130	1.130	1.130	1.130	1.130	1.150
Al_2O_3	0.510	0.510	0.510	0.510	0.510	0..520
SiO_2	0.380	0.390	0.390	0.390	0.380	0.390
TiO_2	0.190	0.190	0.190	0.190	0.190	0.190
La_2O_3	–	–	–	0.005	0.014	0.012
Ce_2O_3	–	–	–	0.019	0.031	0.026
Gd_2O_3	–	–	–	0.004	0.011	0.009
Tb_2O_3	–	–	–	0.060	0.004	0.003
Dy_2O_3	–	0.600	0.353	0.586	0.160	0.133
Ho_2O_3	–	–	–	0.088	0.110	0.090
Y_2O_3	6.960	5.900	5.820	5.270	5.990	4.950
Er_2O_3	–	–	0.345	0.186	0.250	0.204
Yb_2O_3	–	–	–	0.056	0.016	0.013
Y_2O_3 + RE	6.960	6.560	6.550	6.310	6.590	5.440
RE	0.000	0.660	0.698	1.040	0.600	0.490

has ~7.0% (Y). Compositions 4 and 5 have dysprosium and erbium, respectively, as the RE with higher concentration. Composition 2 was prepared as a reference for composition 4, and composition 3 was a reference for composition 5. Composition 1, prepared from 99.9% pure yttria, was a reference for all samples, especially for sample 2, because the ionic radius of Dy^{3+} is very close to that of the Y^{3+} ion, according to Shannon [45]. All compositions are cubic during sintering at 1600 °C and cubic with a low fraction of tetragonal phase at room temperature according to the ZrO_2–Y_2O_3 phase diagram of Chaim *et al.* [40]. The XRD and dilatometry measurements do not detect the monoclinic phase in compositions 1–5, but compositions 6 and 7 have 23% and 38% of the monoclinic phase, respectively, after having been submitted to the same heat treatment as samples of compositions 1–5. The XRD spectra were the same for compositions 1–5 and characteristic of the cubic phase. However, a small fraction of the tetragonal phase, not detected by XRD, must be present; we estimate that to be ~5% for compositions 1 [40] and a little higher for compositions 2–5. In fact, the optical and scanning electron micrographs show the presence of the tetragonal phase precipitates in all compositions. The density measurements of compositions 1–5 gave the following results as the percentage of their theoretical density: 90%, 91%, 92%, 93%, and 94%, respectively. From the microstructures it is seen that composition 1 has a much larger number of grain pores than composition 5. This matched the trend of the density measurements. The porosity influence on the electrical conductivity has been studied by Pascual *et al.* [10] who found that there is no effect when the porosity is smaller than 15%. The maximum porosity of our samples is lower than this value, and the difference between them is even smaller. Therefore, we will assume that the observed difference in conductivity among our samples is not influenced by porosity.

3.2. Conductivity measurements

The impedance spectra of compositions 1–5 have well-defined grain, grain-boundary, and electrode contributions. Fig. 1 shows the impedance spectra for compositions 3 and 5. Compositions 6 and 7 have a more complex spectra with mixed grain and grain-boundary contributions while yet allowing the measurement of σ_t. The σ_g, σ_{gb}, and σ_t temperature dependence are very well described by the Arrhenius equation $\sigma T = A \exp(-E/KT)$ in the temperature range 550–900 K. Experimental points are shown only in Fig. 2. Points taken from the literature are shown for comparison in Fig. 3. Experimental points from compositions 6 and 7 do not fit the Arrhenius equation well and will not be considered further; however, they gave a good indication of the strong effect of the 23% of the monoclinic phase on the conductivity. Parameters of the Arrhenius equation, A and E, are shown in Table III together with recalculated data from the literature. Table IV shows the conductivities from several other works compared with our data from composition 5. The grain conductivity for composition 5, σ_{g5} is 3.5 times higher than σ_{g1} and nearly the same as for the high-purity samples of the literature; but it is 10 times less than the yttria–scandia-doped sample [43], Table IV. The grain-boundary conductivity of composition 5, σ_{gb5}, is also 3.5 times higher than σ_{gb1} and higher than any other reported value in the literature. Taking into account the purity of the starting materials, the concentration of stabilizing ions and the powder processing used to prepare our samples, the high value found for σ_{gb5} is surprising. The activation energy, E_g, shows little variation among our samples but is significantly lower than E_g for samples with higher yttria concentration. Values for E_{gb} are higher than E_g as usual but are near the same value as σ_{gb} for pure samples, Table III.

In order to compare better the σ_g variation among our samples, the following calculations were performed. The σ_g for samples 2–5, σ_{gx}, was approximated by the first-order correction for concentration variation Δc_x by $\sigma_{gx} = \sigma_{g1} - \Delta c_x \, d\sigma/dc$. We used $d\sigma/dc$ from Kuwabara *et al.* [5] and Δc_x, the difference in yttria concentration relative to sample 1. A similar correction was performed considering the influence of the ionic radius on σ_g taking $d\sigma/dr$ from Stafford *et al.* [2]. These calculated values expressed as σ_{gx}/σ_{g1} are shown in the bottom row of Table V. The same ratios, in this case directly calculated from the experimental data, Fig. 3, at 833 °C are shown in the top row. From this table it can be concluded that the influence of the RE on the conductivity is an indirect effect and therefore must be looked for in the

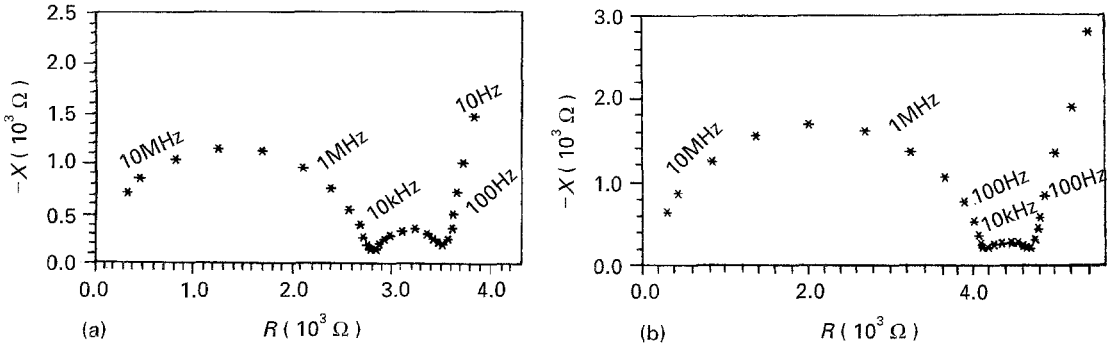

Figure 1 Complex impedance plots measured in air: (a) composition 3 at 398 °C; (b) composition 5 at 409 °C.

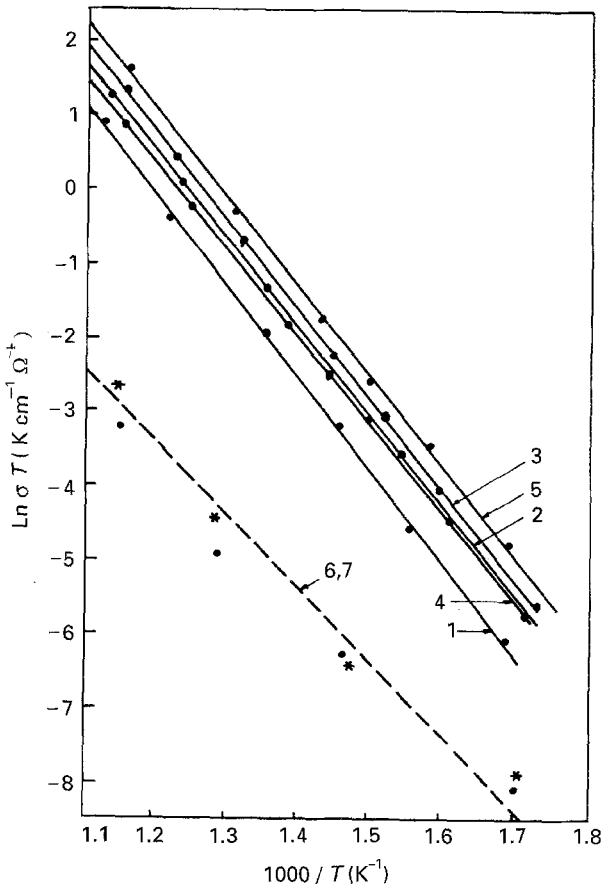

Figure 2 Arrhenius plots for the total conductivity, σ_t, for compositions 1–7. Stars are for composition 6.

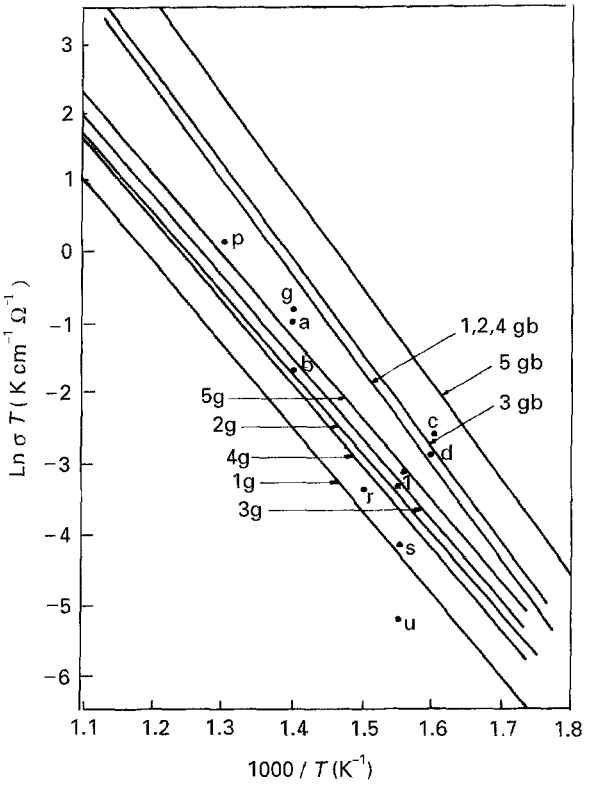

Figure 3 Arrhenius plots for grain (g) and grain-boundary (gb) conductivity for compositions 1–5. Points are from the literature (see Table IV).

microstructural development of each composition. Considering that alumina and silica are impurities that decrease both σ_g and σ_{gb}, their concentration in the grain and grain boundary must have been lowered on going from compositions 1–5. The scavenger effect of the alumina on silica, as found by Butler and Drennan [27], already contributes to the electrolyte cleaning without the presence of the RE ions. We consider that the only possible influence of the RE ions must be made through the difference between their ionic radii and that of the Y^{3+} ions. If this assumption is correct, the influence of Dy^{3+} must be the smallest; that is, the conductivity of composition 2 must be the closest to composition 1 because the Dy^{3+} ion is only 0.8% larger than the Y^{3+} ion, while Er^{3+} is 1.5% smaller according to Shannon [45]. Taking the misfit $\Delta r/r$ of each RE ion relative to the Y^{3+} ion and its respective molar concentration, c_i, the total size misfit, $\Sigma c_i(\Delta r_i/r)$, was calculated for compositions 2–5 and is shown in Table VI. From this table the samples can be divided into two groups: compositions 2 and 4 having RE ions larger than the Y^{3+} ion, and compositions 3 and 5 having the smaller ones. From the conductivity measurements, compositions can also be classified in the same two groups. Therefore, it seems that the smaller RE ions have a larger influence on the segregation of impurities.

3.3. Microstructures

The evolution of microstructures during sintering was studied by optical microscopy in time intervals of 2 h as shown in Fig. 4. The following common features among the compositions were observed: grain pores,

TABLE III Activation energy, E(eV) and pre-exponential, A ($10^6\ \Omega^{-1}\ cm^{-1}$), for σ_g, σ_{gb}, and σ_t from the Arrhenius equation (see Table IV)

	This work					Literature (see last columm Table IV)				
	1	2	3	4	5	A	B	C	D	E
E_g (eV)	1.02	0.98	1.00	1.00	1.00	1.09	1.13	1.13	1.04	1.06
$A_g(10^6\Omega^{-1}cm^{-1})$	1.20	1.50	2.30	1.70	3.50	12.0	12.0	9.0	5.60	6.10
E_{gb} (eV)	1.17	1.17	1.16	1.17	1.18	1.18	1.15	1.15	1.18	1.24
$A_{gb}(10^6\Omega^{-1}cm^{-1})$	312	312	378	312	410	240	210	35	220	250
E_t (eV)	1.05	1.01	1.03	1.01	1.04	–	–	–	–	–
$A_t(10^6\Omega^{-1}cm^{-1})$	1.80	1.90	3.40	2.10	5.50	–	–	–	–	–

TABLE IV Electrical conductivities from the literature (recalculated) compared with composition 5 of this work. (g = grain; gb = grain boundary)

Reference	Sintering temp. (°C)	Stabilizer (mol %)	Impurities (mol %)	Ln σT (Ω^{-1} cm^{-1})	$10^3/T$ (K^{-1})	Ln σT (Ω^{-1} cm^{-1}) Composition 5, This work	See Fig. 2	See Table III
34	1700	10.0 Y_2O_3	–	− 0.95 (gb)	1.40	+ 0.85 (gb)	a	–
34	1600	10.0 Y_2O_3	–	− 1.20 (gb)	1.40	+ 0.85 (gb)	b	–
34	1900	10.0 Y_2O_3	–	− 0.80 (gb)	1.40	+ 0.85 (gb)	g	–
8	1900	10.1 Y_2O_3	–	− 2.90 (gb)	1.60	− 1.90 (gb)	d	B
8	1900	10.1 Y_2O_3	–	− 4.72 (gb)	1.60	− 3.60 (gb)	–	B
8	1500	10.0Y_2O_3	2.2 SiO_2	− 4.18 (gb)	1.55	− 1.20 (gb)	s	C
8	1500	10.0 Y_2O_3	2.2 SiO_2	− 3.35 (gb)	1.50	− 2.40 (gb)	r	C
25	1700	8.0 Y_2O_3	–	− 2.60 (gb)	1.60	− 1.90 (gb)	c	D
25	1700	8.0 Y_2O_3	–	+ 0.20 (g)	1.30	− 0.10 (gb)	p	D
25	1700	8.0 Y_2O_3	0.40 Al_2O_3	+ 1.90 (g)	1.14	+ 1.80 (gb)	–	E
25	1700	8.0 Y_2O_3	0.40 Al_2O_3	+ 2.90 (gb)	1.14	+ 5.80 (gb)	–	E
11	2000	7.75 Sc_2O_3	–	+ 1.20 (g)	1.20	+ 1.10 (g)	–	–
2	1600	12.0 Yb_2O_3	–	− 3.35 (g)	1.55	− 3.00 (g)	t	–
2	1600	12.0 Gd_2O_3	–	− 5.20 (g)	1.55	− 3.00 (g)	u	–
15	1650	4.0 Y_2O_3 + 4.0 Yb_2O_3	–	+ 1.24 (g)	1.14	+ 1.80 (g)	–	–
33	1676	8.9 Y_2O_3	–	− 1.17 (g)	1.38	− 1.00 (g)	–	A
33	1676	8.9 Y_2O_3	–	+ 0.05 (gb)	1.40	+ 0.85 (gb)	–	A
26	1460	9.3 Y_2O_3	–	− 0.52 (g)	1.29	0.00 (g)	–	–
26	1460	9.3 Y_2O_3	–	− 0.28 (gb)	1.29	+ 2.30 (gb)	–	–
45	1750	3.0 Y_2O_3 + 5.0Sc_2O_3	–	+ 3.45 (t)	1.20	+ 1.10 (t)	–	–

TABLE V Grain conductivities ratios at 833 K

σ_{g2}/σ_{g1}	σ_{g3}/σ_{g1}	σ_{g4}/σ_{g1}	σ_{g5}/σ_{g1}
1.80[a]	2.10[a]	1.70[a]	3.00[a]
0.92[b]	0.93[b]	0.89[b]	0.95[b]

[a] Data from Fig. 2.
[b] σ_g corrected for concentration variation $\Delta\sigma/\Delta c$ [5] and RE radii $\Delta\sigma/\Delta r$ [2].

TABLE VI Total size misfit, $\Sigma\, c\Delta r/r$ relative to Y^{3+} radius for each composition

	Composition				
	1	2	3	4	5
$\Sigma\, c\Delta r/r$ (mol %)	0.0	+ 0.5	− 0.2	+ 0.3	− 0.1

$\Delta r/r = [r\,(RE^{3+}) - r\,(Y^{3+})]/r(Y^{3+})$
c = RE molar concentration

grain-boundary pores, and impurity phases at triple points and grain boundaries. Observation of the sintering process was also followed by SEM for some samples. Grain pores were in the largest number in composition 1 decreasing to the lowest value for composition 5. The impurity phase along the grain boundaries grows in the first 4 h sintering and decreases thereafter. The impurity phase at triple points is already well developed in the first 2 h sintering. Composition 5 shows a clean grain boundary at the end of the sintering process. The phase development at the grain boundary and its further cleaning is less pronounced in composition 1.

The average grain size of all compositions after 8 h sintering was almost the same: 25 μm and ranging from 12–45 μm . The scanning electron micrographs, in Fig. 5, show details of the microstructure – a precipitate-free zone in the grain along the grain boundary, grain precipitates, pockets, triple points and clean grain boundaries. The triple points and pockets were EDS analysed and found to be rich in aluminium, and aluminium and silicon, respectively, as shown in Fig. 6. The signals found for zirconium and yttrium are likely to be contributions from the matrix grains. Iron and gold signals are from equipment and sample preparation, respectively. The precipitate phase on the matrix grains we attributed to the small percentage of tetragonal phase from the transformation cubic → tetragonal that occurred during sample cooling, according to the observations of Chaim *et al.* [40]. The precipitate-free zone has already been observed by the same authors in a 12 wt % Y_2O_3–ZrO_2 system and by Buttler and Heuer [39] in calcium and magnesium partially stabilized ZrO_2. This zone is a common feature of compositions 2–5, while in composition 1 the concentration of tetragonal precipitates was lower, making it difficult to observe. The EDS analysis of this zone has shown only zirconium and yttrium. However, the EDS analysis was not sensitive enough to detect the low level of titanium and rare-earths in any region of the microstructure such as grains and grain boundaries.

From the results described above, the following conclusions can be drawn. During grain growth alumina is preferentially segregated to triple points, possibly the larger particles. Silica and alumina fine particles are partially dissolved in the lattice due to the high rate of grain growth, and partially segregated at the grain boundaries. The dissolved fraction is

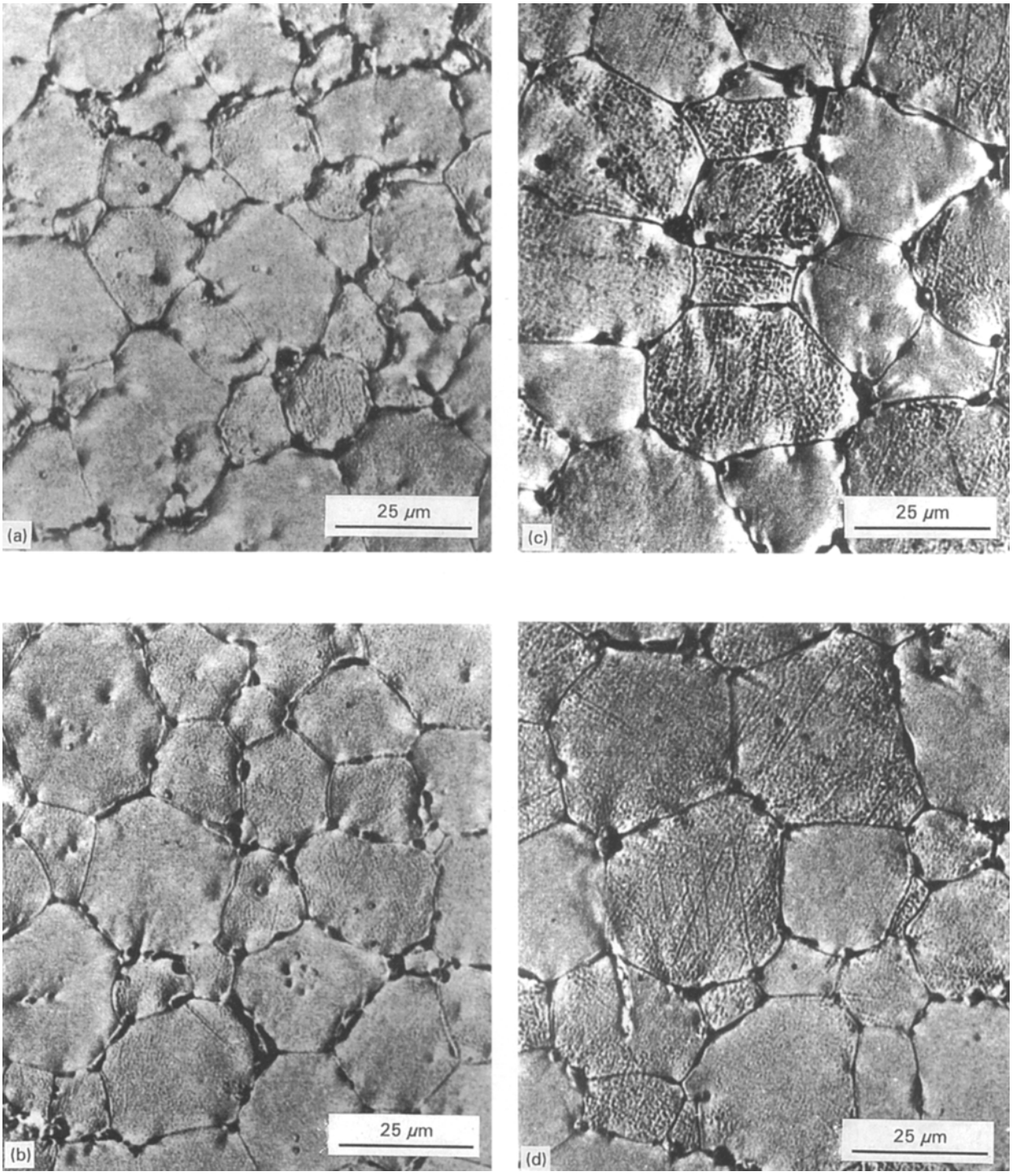

Figure 4 Optical micrographs of the microstructure of composition 5 during sintering: (a) 2 h; (b) 4 h; (c) 6 h; (d) 8 h.

dependent on the RE present in the sample. With further sintering time, when the grain-growth rate has slowed, the segregation of silica and alumina is more efficient. In this stage, the phase at the grain boundaries goes to grain-boundary pockets, pores, and triple points. The influence of the RE is also noticeable on the grain-growth rate in the early sintering stages, decreasing the concentration of pore grains in composition 5 compared with composition 1. Therefore, the electrical conductivity of our samples is a consequence of the process described above – grain and grain-boundary cleaning of alumina and silica.

However, it remains to be discussed how the rare-earths minority ions have such an influence on the microstructural development. As already mentioned, the only relevant difference between the Y^{3+} ion and the RE^{3+} ions is the ionic radius. Smaller and larger RE ions than the Y^{3+} ion will generate an additional size misfit in the matrix when a substitution occurs. The elastic energy due to this misfit may consequently change the segregation of other solutes in these multiple solute samples. The driving force for the segregation process is of an elastic nature only because the Y^{3+} and RE^{3+} ions have the same electrical character.

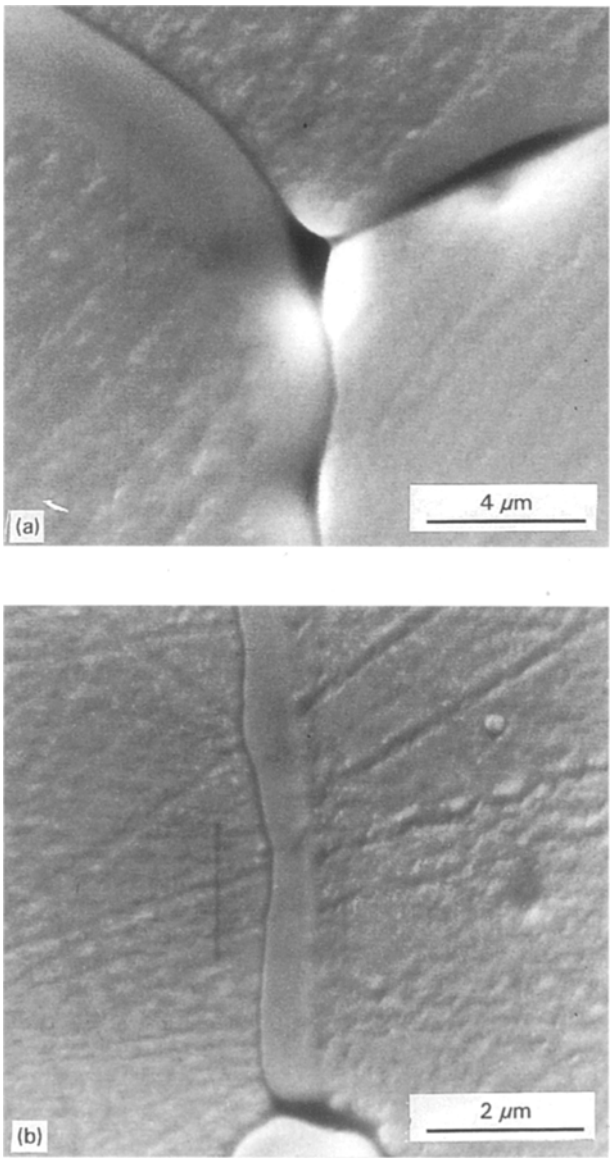

Figure 5 Scanning electron micrograph showing "tweed"-type structure in the grains of two samples from composition 5: (a) selected-area showing pockets, triple point and a precipitate-free zone along the border of the left grain; (b) precipitate-free zone, 0.5 μm thick.

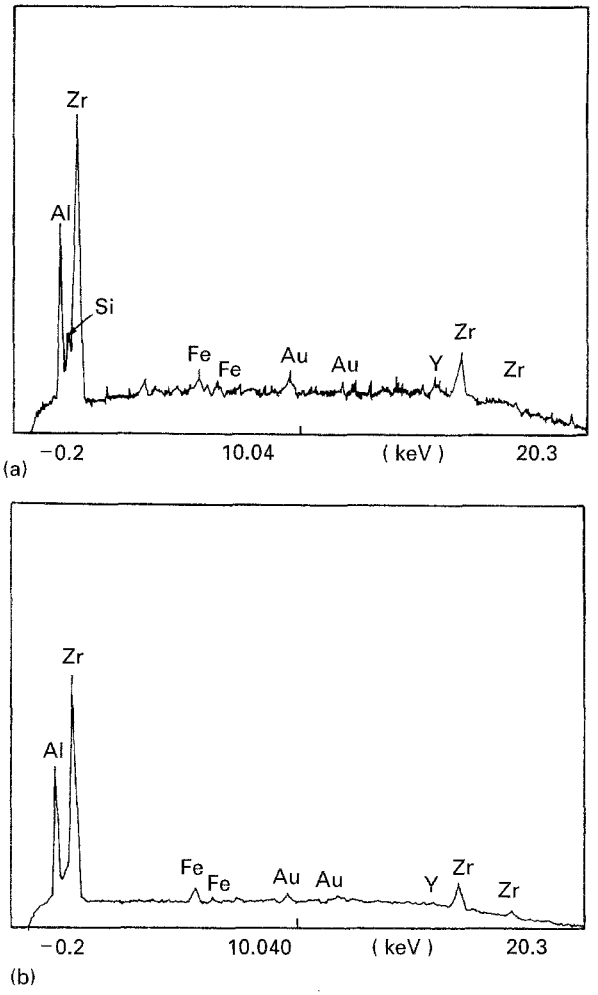

Figure 6 EDS qualitative analysis of selected areas of the microstructure for composition 5: (a) pocket in the grain boundary; (b) a triple point.

The influence of the rare-earths must, therefore, occur at the grain interface. The solute segregation at ceramic interfaces by elastic, electric, and dipole force fields has been studied by Yan *et al.* [38]. Numerical calculations were performed by these authors for the segregation of Ca^{2+}, a majority solute, and Mg^{2+}, a minority solute, in KCl. Their results show a strongly increased segregation of the Mg^{2+} ions at the interface due to Ca^{2+} ions. A similar behaviour is expected in our ceramic electrolytes resulting in the increased segregation of the smaller impurity ions such as Al^{3+} and Si^{4+} to the grain boundaries. The grain-boundary enrichment with silicon increases σ_g and provides the necessary amount of silica for the dewetting of the grain-boundary phase with a consequential increase in σ_{gb}. In addition, according to Chaim *et al.* [40], this silica-rich grain-boundary phase is necessary to produce the precipitate-free zone. In the model proposed by these authors, yttria enrichment of the grain boundary is also necessary, but it was not found in our measurements. It should be noted that the precipitate-free zone of our samples can be as thick as 2 μm, while in the work of the above authors [40] it is 0.1 μm.

Calculations involving a large number of solutes, as in our samples, would be tedious and difficult. However, a detailed analysis of the interface and grain boundary of new samples neodymium- and ytterbium-doped are underway using transmission electron microscopy (TEM) and precision microanalysis.

The dewetting of silica from the grain boundaries, even in electrolytes where its concentration is very low, was observed by Badwall and Drennan [34]. Also highly conductive grain boundaries have been measured in samples stabilized by low radius ions, as is the case for the Y_2O_3–Sc_2O_3 samples studied by Ciachi and Badwal [43]. The total conductivity, σ_t, found by these authors for the system ZrO_2 + 3 mol % Y_2O_3 + 5 mol % Sc_2O_3 and $\ln \sigma_t\ T = 3.45\ \Omega^{-1}\,cm^{-1}$ at 833 K. Therefore, this is also the minimum value for σ_{gb}, nearly the same as σ_{gb5}.

4. Conclusion

The electrical conductivity and microstructure of the multisystem ZrO_2–Y_2O_3–RE_2O_3 (Al_2O_3, SiO_2, TiO_2 impurities) were investigated.

For an Y_2O_3–RE_2O_3 concentration of 12 wt% (~6.5 mol %), the system exhibited a cubic matrix with tetragonal precipitates. Monoclinic phase is also present only in compositions where the Y_2O_3–RE_2O_3 concentration is 10 wt % or lower. The electrical conductivity of the monoclinic phase-free samples is very close or higher than that of electrolytes prepared from high-purity zirconia. The observed influence of the RE ions among our samples cannot be explained in terms of the differences in sample porosities [10] or the beneficial influence of the RE of small ionic radius in pure zirconia [2].

It is considered that the way through which the RE ions would enhance the ionic conductivity is by increasing segregation of impurities. One result of the impurity segregation is the growth of clean grains. The other is a grain-boundary phase capable of migrating to pockets, grain-boundary pores, and triple points. We believe the elastic field generated by the size misfit of RE ions in the ZrO_2–Y_2O_3 matrix may increase the segregation of the small radius impurity ions. This is supported by: (1) calculations done by Yan *et al.* [38] in KCl on the enhanced segregation of Mg^{2+} ions by Ca^{2+} ions; (2) formation of a precipitate-free zone in the interface region of the growing grain – an indication according to Chaim *et al.* [40] that enough silica has been segregated to produce a viscous phase in the grain boundary during grain growth; (3) the reduced porosity of the Y_2O_3–RE_2O_3-doped samples and consequently a smaller grain-growth rate in the early sintering stage than in the sample doped only with Y_2O_3.

Although RE ions with ionic radii larger than the Y^{3+} ion have a beneficial effect on the segregation of impurities (Dy^{3+}), our results seem to indicate that a smaller ionic radius (Er^{3+}) has a more pronounced influence. Coincidentally, it has been found in the literature that small rare-earth ions such as Sc^{3+} in a ZrO_2–Y_2O_3–Sc_2O_3 system [43] increase not only the grain conductivity but also the grain-boundary conductivity (Table IV).

Acknowledgements

The financial support from the FAPESP and CNPq is gratefully acknowledged.

References

1. H. KANEKO, F. JIN and H. TAIMATSU, *J. Am. Ceram. Soc.* **76** (1993) 793.
2. R. J. STAFFORD, S. J. ROTHMAN and J. L. ROUTBORT, *Solid State Ionics* **37** (1989) 67.
3. S. P. S. BADWAL, *J. Mater. Sci. Lett.* **6** (1987) 1419.
4. S. IKEDA, O. SAKURAI, K. UEMATSU, N. MIZUTANI and M. KATO, *J. Mater. Sci.* **20** (1985) 4593.
5. M. KUWABARA, T. MURAKAMI and M. ASHIZUKA, *J. Mater. Sci. Lett.* **4** (1985) 467.
6. S. P. S. BADWAL and M. V. SWAIN, *ibid.* **4** (1985) 487.
7. N. BONANOS, R. K. SLOTWINSKI, B. C. STEELE and E. P. BUTLER, *ibid.* **3** (1984) 245.
8. S. P. S. BADWAL, *J. Mater. Sci.* **19** (1984) 1767.
9. A. I. IOFFE, D. S. RUTMAN and S. V. KARPACHOV, *Electrochim. Acta* **23** (1978) 141.
10. C. PASCUAL, J. R. JURADO and P. DURAN, *J. Mater. Sci.* **18** (1983) 1315.
11. S. P. S. BADWAL, *ibid.* **18** (1983) 3117.
12. *Idem, ibid.* **22** (1987) 4125.
13. T. M. GUR, I. D. RAISTRICK and R. A. HUGGINS, *Mater. Sci. Eng.* **46** (1980) 53.
14. M. F. TRUBELJA and V. S. STUBICAN, *J. Am. Ceram. Soc.* **74** (1991) 2489.
15. G. S. CORMAN and V. S. STUBICAN, *ibid.* **68** (1985) 174.
16. W. WEPNER, *Solid State Ionics* **52** (1992) 23.
17. S. P. S. BADWAL, *Appl. Phys. A* **50** (1990) 449.
18. *Idem, Solid State Ionics* **52** (1992) 23.
19. S. P. S. BADWAL, F. F. CIACHI and R. H. J. HANNINK, *ibid.* **40/41** (1990) 882.
20. D. W. STRICKLER and W. G. CARLSON, *J. Am. Ceram. Soc.* **48** (1965) 286.
21. R. A. PARIS and G. PARIS, US Pat. 3573107, 30 March 1971.
22. H. BERNARD and J. C. VIGUIE, French Pat. 2475531, 8 February, 1980.
23. R. BOSCH GMBH, Br. Pat. 1591781 17 May, 1978.
24. K. C. RADFORD and R. J. BRATTON, *J. Mater. Sci.* **14** (1979) 59.
25. M. MIYAYAMA, H. YANAGIDA and A. ASADA, *Am. Ceram. Soc. Bull.* **64** (1985) 660.
26. M. J. VERKERK, A. J. A. WINNUBST and A. J. BURGGRAAF, *J. Mater. Sci.* **17** (1982) 3113.
27. E. P. BUTLER and J. DRENNAN, *J. Am. Ceram. Soc.* **65** (1982) 474.
28. M. V. INOZEMTZEV and M. V. PERFIL'EV, *Solid Electrolyte Elektrokhim.* **11** (1975) 1031.
29. M. JAYARATNA, M. YOSHIMURA and S. SOMIYA, *J. Mater. Sci.* **22** (1987) 2011.
30. K. KEIZER and A. J. BURGGRAAF, *ibid.* **17** (1982) 1095.
31. M. HARTMANOVA, F. W. POULSEN, F. HANICK, K. PUTYERA, K. D. TUNEGA, A. UROSOVSKAYA and T. V. OROSHNIKOVA, *ibid.* **29** (1994) 2152.
32. A. I. IOFFE, M. V. INOZEMTSEV, A. S. LIPILIN, M. PERFILEV and S. V. KARPACHOV, *Phys. Status Solidi (a)* **30** (1975) 87.
33. M. J. VERKERK, B. J. MIDDELHUIS and A. J. BURGGRAAF, *Solid State Ionics* **6** (1982) 159.
34. S. P. S. BADWAL and J. DRENNAN, *J. Mater. Sci.* **22** (1987) 3231.
35. M. MIYAYAMA and H. YANAGIDA, *J. Am. Ceram. Soc.* **67** (1984) C194.
36. M. MIYAYAMA, H. INOUE and H. YANAGIDA, *ibid.* **66** (1983) C164.
37. M. A. C. G. VAN DE GRAAF, J. H. H. TERMAAT and A. J. BURGRAAF, *J. Mater. Sci.* **20** (1985) 1407.
38. M. F. YAN, R. M. CANNON and H. K. BOWEN, in "Advances in ceramics", Vol. 6, edited by M. F. Yan and A. H. Heuer (American Ceramic Society, Columbus, OH, 1983) p. 255.
39. E. P. BUTLER and A. H. HEUER, *J. Am. Ceram. Soc.* **68** (1985) 197.
40. R. CHAIM, M. RÜHLE and A. H. HEUER, *ibid.* **68** (1985) 427.
41. M. YOSHIMURA, M. YASHIMA, T. NOMA and S. SOMIYA, *J. Mater. Sci.* **25** (1990) 2011.
42. P. LI, I. W. CHEN and E. P. H. JAMES, *J. Am. Ceram. Soc.* 77 (1994) 118.
43. F. T. CIACCHI and S. P. S. BADWALL, *J. Eur. Ceram. Soc.* **7** (1991) 197.
44. B. A. BOUKAMP, in "Equivalent Circuit (EQUIVCRT. PAS.) Users Manual", University of Twente, Department of Chemical Technology, The Netherlands (1989).
45. R. D. SHANNON, *Acta Crystallogra A* **32** (1976) 751.

Received 11 July 1994
and accepted 5 April 1995